International Urogynecology Journal (2023) 34:571–580
https://doi.org/10.1007/s00192-022-05362-8

ORIGINAL ARTICLE

Simulation of the female pelvic mobility and vesical pressure changes employing fluid-structure interaction method

Pouya Zarrinchang[1] · Mahmud Ashrafizaadeh[2] · Nima Jamshidi[3]

Received: 7 June 2022 / Accepted: 5 September 2022 / Published online: 28 September 2022
© The International Urogynecological Association 2022

Abstract

Introduction and hypothesis This study aims to develop a fluid-structural interaction (FSI) method to pinpoint the effects of pressure changes inside the bladder and their impact on the supporting structure and the urethra mobility.

Methods A physiological model of the nulliparous female pelvis, including the organs, supportive structures, and urine, was developed based on magnetic resonance images. Soft tissues with nonlinear hyperelastic material characteristics were modeled. The Navier-Stokes equations governing the fluid flow within the computational domain (urine) were solved. The urine and soft tissue interactions were simulated by the FSI method. The vesical pressure and its impact on the urethral mobility and supportive structures were investigated during the Valsalva maneuver. Moreover, the simulation results were validated by comparing with a urodynamic test and other research.

Results The results demonstrated that the vesical pressure simulated by the FSI method could predict the nonlinear behavior of the urodynamic test pressure. The urethra retropubic bladder neck and the bladder neck-pubic bone angle changed 58.92% and -55.76%, respectively. The retropubic urethral length distance changed by -48.74%. The error compared to the statistical results of other research is < 5%.

Conclusions The total deformation and mobility of the urethra predicted by the FSI model were consistent with clinical observations in a subject. The urethra supports dependence on the tissues' mechanical properties, interaction between the tissues, and effect of urine fluid inside the bladder. This simulation effectively depicts the patterns of urethra mobility, which provides a better understanding of the behavior of the pelvic floor.

Keywords Pelvic floor muscle · Stress urinary incontinence · Fluid-structure interaction · Vesical pressure simulation

Abbreviations

ABD	Abdominal
ATFP	Arcus tendineus fascia pelvis
BN	Bladder neck
CL	Cardinal ligament
Det	Detrusor
FSI	Fluid-structure interaction
IAP	Intra-abdominal pressure
LAM	Levator ani muscle
LLR	Lateral ligaments of the rectum
MPa	Megapascal
MRI	Magnetic resonance imaging
P	Pressure
PFD	Pelvic floor dysfunction
PFM	Pelvic floor muscle
SUI	Stress urinary incontinence
URO	Urodynamic test
USL	Uterosacral ligament
VES	Vesical

✉ Mahmud Ashrafizaadeh
mahmud@iut.ac.ir

[1] Mechanical Engineering group, Pardis College, Isfahan University of Technology, Isfahan 84156-83111, Iran

[2] Department of Mechanical Engineering, Isfahan University of Technology, Isfahan 84156-83111, Iran

[3] Department of Biomedical Engineering, Faculty of Engineering, University of Isfahan, Isfahan, Iran

Introduction

Pelvic floor dysfunction (PFD) can induce stress urinary incontinence (SUI) in women. Due to the prevalence of SUI [1], numerous researchers have proposed several hypotheses over the past decades [2–4]. One of the hypotheses in SUI, the "hammock hypothesis" by DeLancey [4], states that the increase of intra-abdominal pressure (IAP) is transferred to

the pelvic floor. The urethra lies on the endopelvic fascia and the anterior vaginal wall supportive layer. This supporting layer is connected to the pelvic sidewall by arcus tendineus fasciae pelvis (ATFP) and levator ani muscles (LAM). This pressure compresses the urethra to a hammock-like supportive layer and closes the lumen. This support provides the urethral closure with the pressure that should be greater than the IAP to prevent SUI. However, it is essential to mention that further investigation shows that urethral support is not the only reason for SUI and the maximal urethral closure pressure is the strongest factor associated with SUI [5]. Therefore, the urethra closure pressure and the "pressure transmission" are essential in understanding SUI.

On the other hand, the hammock hypothesis exposes the limitations of vivo experiments. For instance, this hypothesis cannot explain why some operations such as mid-urethral sling surgery fail [6]. Biomechanical models implementing medical images do not have the limitations of vivo experiments and deepen the understanding of supportive structures and surgical techniques.

Several finite element modeling simulations of the pelvic cavity have been carried out recently. However, these studies develop limited clinical applications due to subsequent simplifications such as removing critical anatomical structures and disregarding supportive organs [7, 8]. Furthermore, the poor imaging quality of the supporting organs makes it undesirable to establish the boundary conditions and the accurate loading in the research [9, 10]. Various studies have investigated the impairment in the pelvic floor muscles (PFM) and vaginal wall and the effect of impairment on pubourethral, uterosacral (USL), cardinal (CL), and lateral rectal (LLR) ligaments by considering the weakness in the material properties [11, 12]. Despite applying relatively accurate models, some of these studies assumed the ligaments were modeled with linear elements [11], and the urine fluid is also modeled as an elastic solid or not considered [7, 8, 11, 12].

Obviously, specific injuries to individual component structures influence the passive aspects of the urethra closure. Various parameters such as resting and transmission pressures and the rate of abdominal pressure changes are continuous variables due to the presence of the urine and the interaction with the bladder, which accordingly impact the urethra position, supportive layer, and the urethra closure pressure. These parameters are essential and must be considered to demonstrate accurate clinical results.

Due to the lack of reported studies, a nearly realistic pelvic model has been designed and constructed employing magnetic resonance imaging (MRI). Organs and the supporting structures including the pelvic floor muscles, ligaments, and urine have been considered in this model. In addition, a fluid-structure interaction (FSI) model has been developed to simulate the effects of the supportive structures, the presence of the urine inside the bladder, and its effects on the bladder displacement and supports. Moreover, the simulation results of the present study have been compared with and validated against those of some volunteer urodynamic tests as well as those of other simulations and statistical analyses.

Materials and methods

A 3D computational model of the present work was constructed using an MRI of a 23-year-old female with a body mass index (BMI) of 22 kg m^{-2}, who was healthy, nulliparous, and without a history of any previous surgery. A gynecologist rejected any present morphological or functional abnormalities. The authors used the medical information of the volunteer, and this article does not contain any studies with human participants performed by any of the authors. Also, the volunteer has consciously and knowingly agreed for her medical information to be accessed by the researchers, and ethical approval was not required for this computational modeling study.

Pelvic MRI was performed using a 3-Tesla scanner (General Electric, Waukesha, WI, USA) while lying down at rest. A high-resolution (T2-w) pelvic MRI with 1.25 mm slices was obtained. The device's field of view was 436 mm, and the matrix was 256 × 256. High-resolution images were imported to Mimics 17.0 software (Materialise Group, Leuven, Belgium). Under the supervision of an expert, various parts of the pelvic organs and supporting structures were identified, and the thresholds for different tissues were determined to create the closed surfaces for each anatomical structure called the surface masks. The surface masks are converted to the computational volume of all parts' components. Also, the smoothing algorithm was used to smooth the models' surfaces. The 3D model was checked for the surface intersection. The final 3D model includes:

- The pelvic bone.
- All pelvic organs, including the bladder, urethra, vagina, uterus, and rectum.
- The urethral support system including the PFM and pelvic fascia.
- Supportive ligaments of the urethra and uterus, CL, USL, ATFP, and LLR.
- Urine.

The anatomical characteristics of the constructed geometry were validated by other studies such as [13–15], and an expert confirmed the final 3D model. Figure 1 illustrates a final biomechanical pelvic model including all the above structures for simulations.

Fluid and solid domains were discretized by unstructured tetrahedral meshes. Mesh sensitivity analysis was performed by ANSYS Fluent meshing 2019 R3 to make the mesh

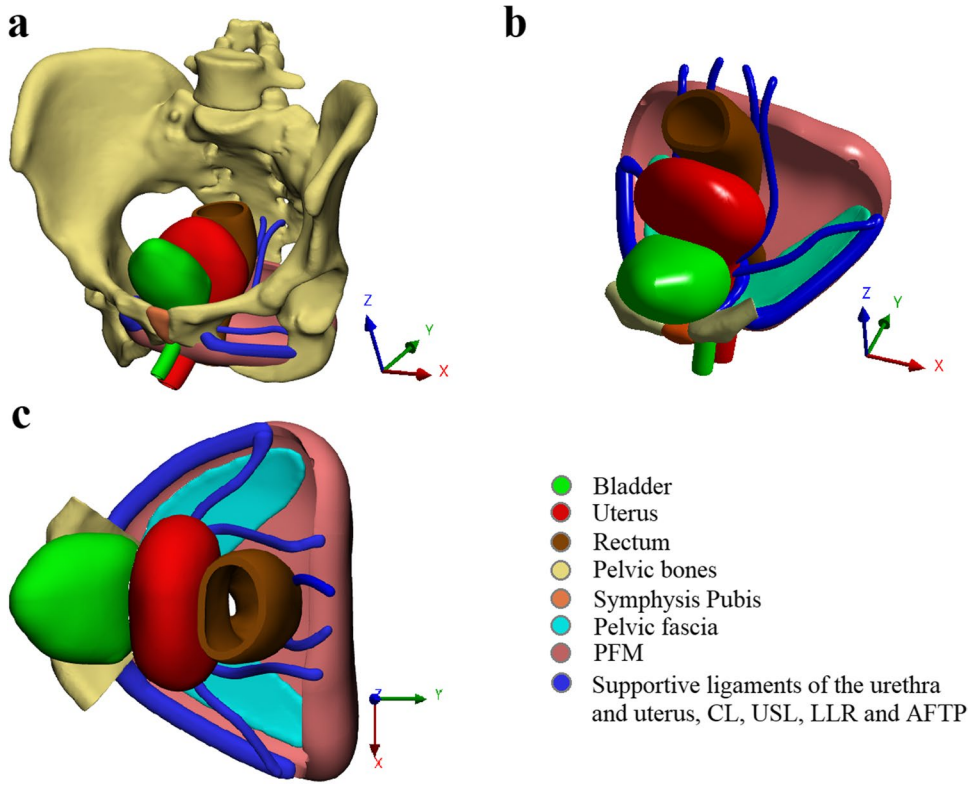

Fig. 1 Anatomical representation of the biomechanical model based on the MR images. **a**, **b** Isometric and **c** axial views of the pelvic bone, organs, and support structures

independent and validate the results. Four different grids were created for the fluid domain with 861,514, 1,013,546, 1,672,351, and 2,158,852 elements. It was observed that the pressure change at the center of the bladder in time step 0.08 s during the Valsalva maneuver between the two finest meshes was < 1%. Therefore, the mesh with 1,672,351 elements was selected for appropriate precision and to avoid high computational costs. Additionally, a mesh in the same order with 1,149,846 elements was created for the solid domain to establish the solution accuracy in the fluid and solid field interaction. Figure 2 reveals the unstructured mesh in fluid and solid domains.

Fluid domain

Urine was considered an incompressible Newtonian fluid with a density of 1030 kg m^{-3} and a viscosity of 7.97×10^{-4} kg m^{-1} s^{-1} at 37 °C [16]. The transient laminar urine flow regime inside the bladder was calculated using the Navier-Stokes incompressible 3D equations [17, 18]. The governing equations, continuity, and momentum equations are defined as:

$$\nabla.\mathbf{u}_f = 0$$

$$\rho \frac{D\mathbf{u}_f}{Dt} = -\nabla P + \nabla \times \tau + f$$

In this equation, **u** is the velocity vector, τ is the stress tensor, P is the pressure tensor, f is the force on the fluid, and ρ is the fluid density [17, 18]. Boundary conditions must be carefully selected to provide realistic results. For this purpose, the bladder was considered full of urine at the beginning of the simulation. In the FSI simulation, the entire outer surface of urine was considered as the wall of the interaction between the fluid and the structure. The outflow boundary condition was also utilized at the bladder outlet.

Solid domain

The first step in accurately modeling the soft tissue of pelvic organs and supporting structures is to select an appropriate model for material properties. Many experiments have been performed on human tissue properties, and it has been found that nonlinear hyperelastic models provide the best accurate prediction of soft tissue material properties. The stress-strain relationship is typically derived from the strain energy for hyperelastic materials. The first derivative of the strain energy function relative to strain was employed to evaluate the stress [17, 18]:

$$\sigma_S = \frac{\partial W}{\partial E_{ij}}$$

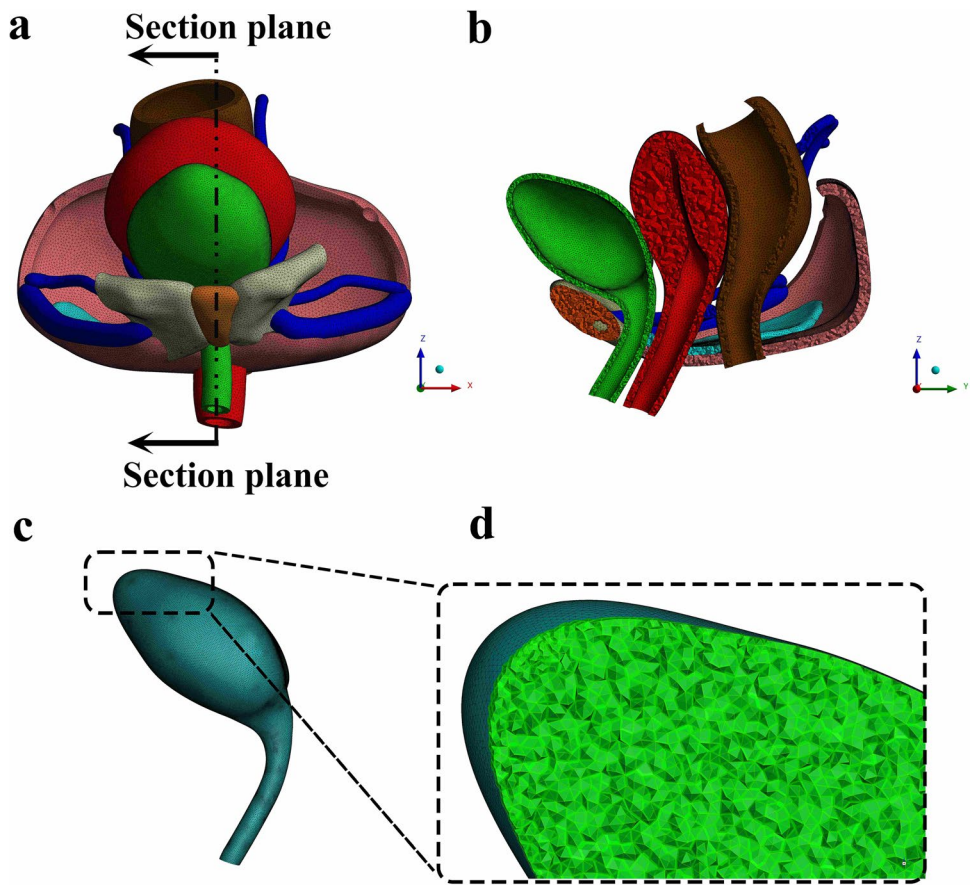

Fig. 2 Computational mesh domains. **a**, **b** Coronal and midsagittal section plane views of the solid parts. **c** Fluid part (urine) and **d** midsagittal section plane of the urine mesh

where σ_S is the Cauchy stress tensor in the solid domain, E_{ij} Green's strains, and W the strain energy density.

Experimental data have been used to model different tissue material properties [19–23]. The curve-fitting algorithm extracts appropriate hyperelastic models based on the present experimental data. The curve fitting results demonstrate that Ogden's [24] and Yeoh's [25] models adhere to the best agreement with the experimental results. The strain energy density of Ogden and Yeoh's models proposed the following:

$$W(\lambda_1, \lambda_2) = \sum_{P=1}^{n} \frac{\mu_P}{\alpha_P}({\lambda_1}^{\alpha_p} + {\lambda_2}^{\alpha_p} + {\lambda_1}^{-\alpha_p}{\lambda_2}^{-\alpha_p} - 3)$$

$$W = \sum_{i+j=1}^{\alpha} C_{ij}(I_1 - 3)^i + (I_2 - 3)^j$$

where λ_j are principal stretches with $i, j = 1, 2$. μ_P 'α_P, C are the material constants, and I is the strain invariant. Also, the bones are considered linear elastic materials [7].

Table 1 presents the calculated curve fitting parameters of the hyperelastic models used for different structures.

Thirty-five different contact constraints determine the relationship among all tissues. The bonded constraint type connects ligaments to the pelvic organs and the pelvic floor muscle to the pelvic fascia. In addition, the connection between other tissues was frictionless. The pelvic bone and supportive ligaments of the urethra and uterus, USL, CL, ATFP, and LLR attached to the pelvic bone were fixed. The entire surface inside the bladder was considered the FSI boundary, and the lateral movement of the bladder, vagina, and rectum was limited. IAP values were extracted from the volunteer's urodynamic test. Since MRI imaging was performed while the volunteer was supine, at rest, and different from the urodynamic test position, it was necessary to correct the amount of IAP applied in the simulation. For this purpose, the average IAP of the volunteer at rest (5.78 cmH_2O) was subtracted from the IAP of the Valsalva maneuver of volunteer urodynamic test results. The maximum IAP of about 40 cmH_2O was calculated, consistent with Noakes et al. [26]. Standard gravity acceleration ($g = 9.8066\ m.s^{-2}$) was also applied to the FSI solution.

Solution method

The effect of urinary fluid on pelvic organs and the supporting structures was simulated by strongly coupled two-way FSI in ANSYS 2019 R3. The two-way method applied the structural changes on fluid. The reactions of fluid are also applied to the structure. The strong coupling means solving each time step more than once to obtain more accurate results. Fluent for fluid flow with finite volume method and

Table 1 Properties of hyperelastic materials and models made from experimental data

Organs and supportive structures	α_1	μ_1		Model	Experimental data
Bladder and urethra	2.55	0.14		Ogden	Chantereau et al. [19]
Rectum	13.23	0.064		Ogden	Rubod et al. [20]
Vagina and uterus	12.26	0.15		Ogden	Rubod et al. [20]
Pelvic ligaments (ATFP, CL, LLR, USL)	10.73	0.59		Ogden	Rivaux et al. [21]
Supportive ligament of the urethra	10.86	0.29		Ogden	Rivaux et al. [21]
	C_{10}	C_{20}	C_{30}	Model	Ref.
Pelvic fascia	0.93	-0.64	0.5	Yeoh	Jelen et al. [22]
Pelvic floor muscles	0.032	0.032	0.035	Yeoh	Janda [23]
	Young's modulus	Poisson's ratio	Density	Model	Ref.
Bones	2130 MPa	0.3	2000	Linear elastic	Cosson et al. [7]

transient structure for the solid domain with finite element method were the solutions that participated in system coupling. The boundary conditions for fluid-structure coupling [17] between the urine and the bladder wall are given by:

$$\sigma_s \mathbf{n}_s = -\sigma_f \mathbf{n}_f$$

$$\mathbf{u}_f = \mathbf{u}_s$$

$$x_f = \mathbf{d}_s$$

where σ_s and σ_f are the Cauchy stress tensor for solid and fluid domains, $\mathbf{n}_s$ and $\mathbf{n}_f$ are normal unit vectors for solid and fluid domains, $\mathbf{u}_f$ and $\mathbf{u}_s = \frac{\partial d_s}{t}$ are the fluid and solid velocity, and x_f and $\mathbf{d}_s$ are the fluid and solid displacement.

Four convergence criteria for the transient structure, fluid flow, data transfer from fluid flow to transient structure, and data transfer from transient structure to fluid flow were obtained at every time step during the simulation.

The "dynamic mesh" implementing the algorithms of "remeshing" and "smoothing" updated the mesh in each time step based on the changes in the boundary of the fluid domain. Volume-based solution stabilization has been utilized to stabilize the convergence.

The Semi-Implicit Method for Pressure-Linked Equations (SIMPLE) algorithm in pressure-based segregated methods was selected. The second-order implicit Euler and the second-order upwind schemes were adopted to achieve the pressure and the momentum discretization of the governing equations, respectively.

Results

Fluid domain

Vesical pressure results and validation

A two-way strongly coupled FSI simulation was performed for the generated mesh. IAP during the Valsalva maneuver was extracted from the volunteer urodynamic test results. The simulation end time and the time step were 0.16 and 0.005 s, respectively.

The simulation results of pressure changes at the center of the bladder ($P_{VES,\ FSI}$) were extracted from the fluid domain and compared with the vesical pressure ($P_{VES,\ URO}$) of the urodynamic test (Fig. 3a). As shown in Fig. 3a, the simulated $P_{VES,\ FSI}$ agrees well with $P_{VES,\ URO}$. Since the simulation employs a strong two-way FSI solution, the convergence would improve with the continuation of the solution.

The difference among $P_{VES,\ FSI}$, and $P_{VES,\ URO}$ is partly due to the value of IAP in the urodynamic test being non-zero at the start. However, the IAP of loading at the beginning of the simulation is forced to be zero to prevent a shock in the computational domain due to the sudden loading effect. Moreover, the 5.78 cmH_2O IAP loading was subtracted because the volunteer position in MRI and the urodynamic test are different. Although the detrusor muscle pressure ($P_{DET,\ URO}$) was not applied in the FSI simulation, the $P_{DET,\ URO}$ is given in Fig. 3a for comparison purposes.

Barzegari et al. [27] calculated the pressure at the center of two simple spherical models. The first model (physiological model) has a supportive structure. Also, the linear elastic model was utilized to simulate material properties. The second model (pathological model) has no supportive structure. In addition, the linear elastic and hyperelastic (Mooney-Rivlin) models were used to simulate material properties.

The present simulated ($P_{VES,\ FSI}$) were compared with those reported by Barzegari et al. [27] because of their initial phase similarities of IAP loading (Fig. 3b). The present $P_{VES,\ FSI}$ has increased from the beginning to 0.05 s and is converged to the physiological model. After that, by increasing the pressure simulation load, the $P_{VES,\ FSI}$ diverged from the physiological model and converged towards the pathological models' results because of the hyperelastic materials model employed.

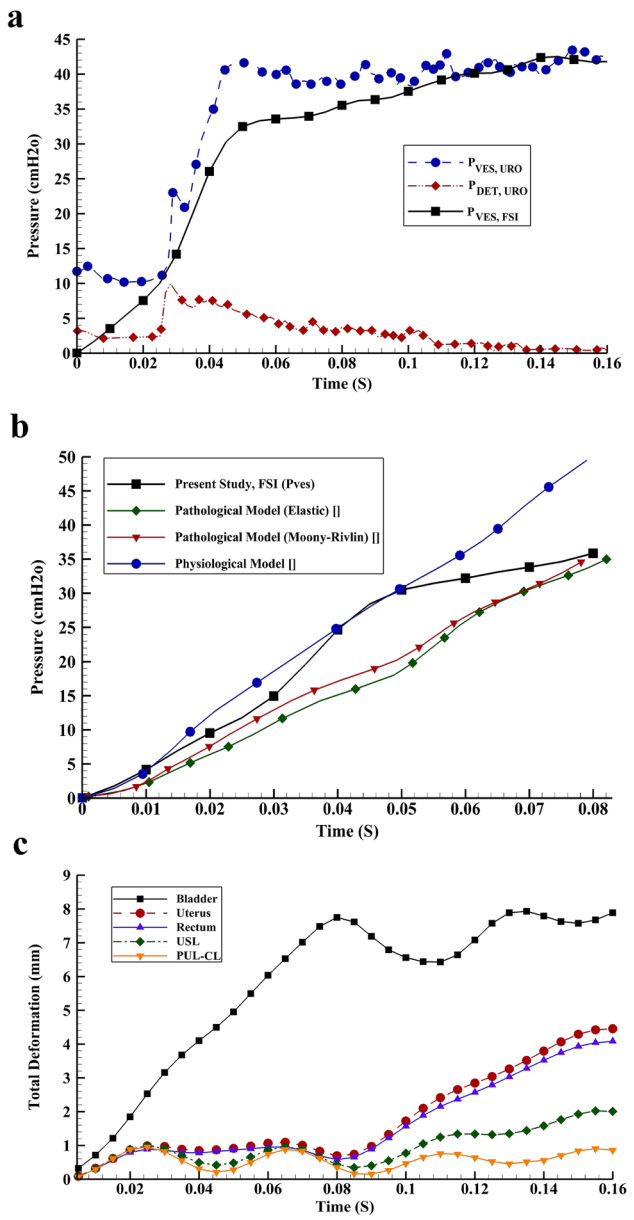

Fig. 3 Validation of pressure changes in the center of the bladder (**a**) Comparison between FSI results and volunteer urodynamic test. (**b**) Comparison of the FSI results and numerical solution of Barzegari et al. [27] and (**c**) total deformations of organs and supportive ligaments

Solid domain

Total deformation and urethra mobility

Based on the FSI simulation results, the bladder, urethra, uterus, vagina, and rectum are exposed to the highest deformation rates. The bladder was compressed 7.8 mm towards the symphysis pubis bone at t = 0.08 S. In addition, the rectum and the uterus are descended 4.08 and 4.45 mm, respectively, at t = 0.016 S. The pelvic floor muscle moves inferior and posterior about 8.44 and 2 mm at t = 0.03 S (Figs. 3c and 4a–e). In addition, despite the minimum changes of the supportive ligaments of the urethra, at the maximum deformation time, the highest concentration of equivalent von Mises stress, about 0.53 MPa, was seen in this area. Since von Mises stress is a combination of normal and shear stresses, the risk of injuries in this ligament is high.

Table 2 illustrates the bladder neck mobility compared with the results of statistical shape modeling by Routzong et al. [28]. The urethral length reduced by 7.58% because of the Valsalva maneuver. The rotation of the bladder neck changed the retropubic bladder neck and the bladder neck-pubic bone angle by 58.92% and -55.76%, respectively. Furthermore, the bladder and urethra were compressed to the symphysis pubis bone. The retropubic urethral length distance was altered by -48.74%. Also, the percentage of errors between these FSI results and the statistical results of Routzong et al. [28] was < 5%, indicating the simulated model's accuracy.

Moreover, the alpha angle defined by Pregazzi et al. [29] is calculated. The alpha angle is between the BN–S line and the midline of the symphysis pubis. The distance from the bladder neck (BN) to the lowest point of the symphysis pubis (S) is also called BN–S line.

The alpha angle at rest was 91° and at the Valsalva maneuver was 108°, which are in a good agreement with those reported by Pregazzi et al. [29] and Brandao et al. [12] (91 vs. 92.0 ± 6.0 and 91.8 at rest, 108 vs. 100 ± 8 and 105.7 at Valsalva maneuver).

Discussion

A nulliparous female pelvic model was constructed based on MRI including the organs, ligaments, supporting structure, and urine. The biomechanical simulation based on the FSI method predicts the pressure changes inside the bladder and urethra mobility. Validation of the fluid simulation results is performed by comparing with both an actual urodynamic test ($P_{VES, FSI}$ vs. $P_{VES, URO}$) and the simulation results of Barzegari et al. [27]. The solid domain results are compared against the statistical results of Routzong et al. [28]. Also, the alpha angle changes are compared by Pregazzi et al. [29] and Brandao et al. [12].

Figure 4 presents the mobility of the pelvic organs during the Valsalva maneuver. Increasing the IAP causes the bladder, uterus, and rectum to move inferior and posterior. The urethra rotates clockwise in the form of a "C" shape

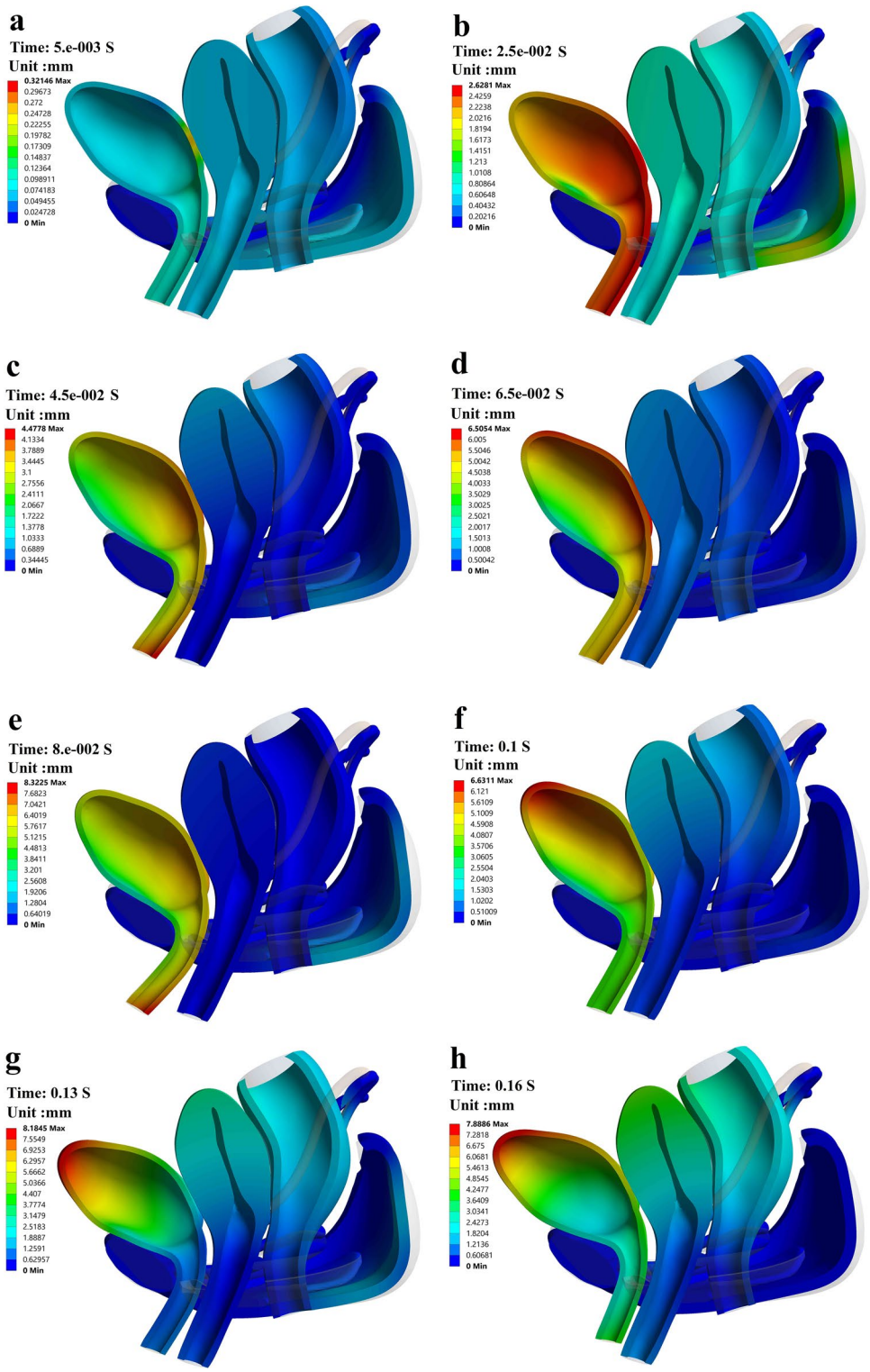

Fig. 4 Total deformation contours. (**a**) t = 0.005 s, (**b**) t = 0.025 S, (**c**) t = 0.45 S, (**d**) t = 0.065 S, (**e**) t = 0.08 S, (**f**) t = 0.1 S, (**g**) t = 0.13 and (**h**) t = 0.16 S

and surrounds the pubic bone [11] (Fig. 4a–e). Despite the increase in IAP, the urethra returns slightly to its first position and rotates in the opposite direction, and the "S" shape was observed [28] because of the hyperelastic mechanical properties of the supporting tissues (Fig. 4f–h).

The findings of the current study indicate that changes in the bladder and urethra's total deformation and mobility rates were neither linear nor simple. As mentioned, the most significant change occurs at t = 0.08 S, and the IAP of simulation loading is 13.86 cmH_2O before reaching the maximum

Table 2 Comparison of bladder neck mobility parameters in the present work with the statistical analysis data of 23 volunteers by Routzong et al. [29]

Variable	FSI simulation (present study)				Dynamic ultrasound measurements (statistical analysis) [29]				Error (%)[1]
	Rest	Valsalva	Change	Change (%)	Rest	Valsalva	Change	Change (%)	
Urethral length (cm)[2]	3.45	3.19	–0.26	–7.53	4.01 ± 0.60	3.60 ± 0.58	–0.41 ± 0.36	–10.22	2.69
Retropubic bladder neck angle (°)[3]	56	89	33	58.92	57.34 ± 23.57	88.33 ± 22.71	30.99 ± 23.58	54.04	4.88
Retropubic urethral length (cm)[4]	1.19	0.61	–0.58	–48.73	2.09 ± 0.68	1.04 ± 0.68	–1.05 ± 0.61	–50.23	1.5
Bladder neck-pubic bone angle (°)[5]	52	23	-29	–55.76	65.40 ± 22.00	28.25 ± 56.81	–37.16 ± 21.27	–56.81	1.05

[1]Difference in % change across FSI simulation (present study) and dynamic ultrasound measurements (statistical analysis) [29]

[2]Urethral length: The distance between the urethral meatus and the opening of the urethra

[3]Retropubic bladder neck angle: The angle between the BN-S line and the line following the superior edge of the symphysis pubis from the S point

[4]Retropubic urethral length: The length of the BN-S line

[5]Bladder neck-pubic bone angle: The angle between the BN-S line and the vertical axes from the S point

IAP of simulation loading. The supporting structure trying to prevent this movement is seen in Fig. 3c. As a result, the pelvic floor mechanism should not be analyzed using simplified simulations, and the FSI simulations are recommended to be utilized to provide accurate findings.

One should note that the present study has its own limitations. First, the simulation model is based on some MRIs of a specific volunteer; hence, it may not be generalized to all cases. However, the authors aimed to establish a method for achieving accurate and realistic results that could alleviate this restriction when compared with available statistical data. Furthermore, this method can be applied to other groups of volunteers in future studies. Second, the LAM in our model differs from anatomical descriptions in the literature regarding origin, insertion, and shape. The effect of these differences is unknown, so our findings should be considered conceptual. It might be better to model the LAM as a combination of puborectalis, pubococcygeus, and iliococcygeus muscles to improve the accuracy. Third, available literature indicates that the supportive ligaments of the urethra and the impairment of these ligaments in SUI patients considerably impact urethral support [12]. On the other hand, as mentioned in the results, the maximum changes in equivalent von Mises stress are observed in supportive ligaments of the urethra area, which is consistent with the literature. However, it is essential to note that this ligament is modeled as a single supporting ligament of the urethra and uterus. It is necessary that the modeling of this part is more accurate and the ligaments are modeled separately and address other connective tissue attachments in this area. Further consideration of these connective tissue attachments of the urethral support might be beneficial to improve the accuracy of the simulations. Fourth, The maximum IAP of about 40 cmH_2O calculated in the Valsalva maneuver is considered for simulation loading pressure in the present study. Still, it is necessary to mention that the research of Fuganti et al. [30] investigated SUI in 319 women. The results show that the cough leading to SUI had a leak point and peak pressures are > 120 and 140 cmH_2O. Therefore, it is recommended that cough IAP pressure of > 150 cmH_2O is simulated in future research.

Despite all the above-mentioned limitations, the authors believe that the present study, which is based on a relatively complete categorical female pelvic model, is a step forward in simulating realistic pelvic organs and their supportive structures.

Conclusions

A model of a 23-year-old female pelvis was generated. The biomechanical simulation was performed by considering the effects of urine on the bladder employing the FSI method. Vesical pressure and its impact on the urethral mobility and supportive structures were investigated during the Valsalva maneuver. It was determined that the total deformation and urethra mobility did not change linearly with increasing IAP. The urethra support and mobility depend on the material properties of the tissues, interaction

among the tissues, and effect of urine fluid inside the bladder. This simulation depicts urethral movement patterns consistent with clinical observations, which is valuable for better understanding the behavior of the pelvic floor.

Authors contributions P Zarrinchang: Data collection, Running the simulation, Project development, Writing the manuscript.

M Ashrafizaadeh: Design and concept of the study, Methodology, Project supervision.

N Jamshidi: Design and concept of the study, Project development, Project co-supervision.

Declarations

Conflicts of interest None.

References

1. Luber KM. The definition, prevalence, and risk factors for stress urinary incontinence. Rev Urol. 2004;6:S3.
2. Enhorning G. Simultaneous recording of intravesical and intraurethral pressure. Acta Chir Scand. 1961;276(Suppl):1–68.
3. Petros PEP, Ulmsten UI. An integral theory of female urinary incontinence: experimental and clinical considerations. Acta Obstet Gynecol Scand. 1990;69:7–31. https://doi.org/10.1111/j.1600-0412.1990.tb08027.x.
4. DeLancey JO. Structural support of the urethra as it relates to stress urinary incontinence: the hammock hypothesis. Am J Obstet Gynecol. 1994;170:1713–23. https://doi.org/10.1016/S0002-9378(12)91840-2.
5. DeLancey JO, Trowbridge ER, Miller JM, Morgan DM, Guire K, Fenner DE, Weadock WJ, Ashton-Miller JA. Stress urinary incontinence: relative importance of urethral support and urethral closure pressure. J Urol. 2008;179:2286–90. https://doi.org/10.1016/j.juro.2008.01.098.
6. Kenton K, Stoddard AM, Zyczynski H, Albo M, Rickey L, Norton P, Wai C, Kraus SR, Sirls LT, Kusek JW. 5-year longitudinal followup after retropubic and transobturator mid urethral slings. J Urol. 2015;193:203–10. https://doi.org/10.1016/j.juro.2014.08.089.
7. Cosson M, Rubod C, Vallet A, Witz J, Dubois P, Brieu M. Simulation of normal pelvic mobilities in building an MRI-validated biomechanical model. Int Urogynecol J. 2013;24:105–12. https://doi.org/10.1007/s00192-012-1842-8.
8. Chen Z-W, Joli P, Feng Z-Q, Rahim M, Pirró N, Bellemare M-E. Female patient-specific finite element modeling of pelvic organ prolapse (POP). J Biomech. 2015;48:238–45. https://doi.org/10.1016/j.jbiomech.2014.11.039.
9. Luo J, Chen L, Fenner DE, Ashton-Miller JA, DeLancey JO. A multi-compartment 3-D finite element model of rectocele and its interaction with cystocele. J Biomech. 2015;48:1580–6. https://doi.org/10.1016/j.jbiomech.2015.02.041.
10. Chen L, Ashton-Miller JA, DeLancey JO. A 3D finite element model of anterior vaginal wall support to evaluate mechanisms underlying cystocele formation. J Biomech. 2009;42:1371–7. https://doi.org/10.1016/j.jbiomech.2009.04.043.
11. Peng Y, Khavari R, Nakib NA, Boone TB, Zhang Y. Assessment of urethral support using MRI-derived computational modeling of the female pelvis. Int Urogynecol J. 2016;27:205–12. https://doi.org/10.1007/s00192-015-2804-8.
12. Brandão S, Parente M, Mascarenhas T, da Silva ARG, Ramos I, Jorge RN. Biomechanical study on the bladder neck and urethral positions: simulation of impairment of the pelvic ligaments. J Biomech. 2015;48:217–23. https://doi.org/10.1016/j.jbiomech.2014.11.045.
13. Albright TS, Gehrich AP, Davis GD, Sabi FL, Buller JL. Arcus tendineus fascia pelvis: a further understanding. Am J Obstet Gynecol. 2005;193:677–81. https://doi.org/10.1016/j.ajog.2005.02.129.
14. Lin M, Chen W, Huang L, Ni J, Yin L. The anatomy of lateral ligament of the rectum and its role in total mesorectal excision. World J Surg. 2010;34:594–8. https://doi.org/10.1007/s00268-009-0371-1.
15 Ashton-Miller JA, DeLancey JO. Functional anatomy of the female pelvic floor. Ann N Y Acad Sci. 2007;1101:266–96. https://doi.org/10.1196/annals.1389.034.
16. Inman BA, Etienne W, Rubin R, Owusu RA, Oliveira TR, Rodriques DB, Maccarini PF, Stauffer PR, Mashal A, Dewhirst MW. The impact of temperature and urinary constituents on urine viscosity and its relevance to bladder hyperthermia treatment. Int J Hyperth. 2013;29:206–10. https://doi.org/10.3109/02656736.2013.775355.
17. Takaddus AT, Chandy AJ. A three-dimensional (3D) two-way coupled fluid-structure interaction (FSI) study of peristaltic flow in obstructed ureters. Int J Numer Methods Biomed Eng. 2018;34:e3122. https://doi.org/10.1002/cnm.3122.
18. Saeedi M, Shamloo A, Mohammadi A. Fluid-structure interaction simulation of blood flow and cerebral aneurysm: Effect of partly blocked vessel. J Vasc Res. 2019;56:296–307. https://doi.org/10.1159/000503786.
19. Chantereau P, Brieu M, Kammal M, Farthmann J, Gabriel B, Cosson M. Mechanical properties of pelvic soft tissue of young women and impact of aging. Int Urogynecol J. 2014;25:1547–53. https://doi.org/10.1007/s00192-014-2439-1.
20. Rubod C, Brieu M, Cosson M, Rivaux G, Clay J-C, de Landsheere L, Gabriel B. Biomechanical properties of human pelvic organs. Urology. 2012;79:968.e917–968.e922. https://doi.org/10.1016/j.urology.2011.11.010.
21. Rivaux G, Rubod C, Dedet B, Brieu M, Gabriel B, Cosson M. Comparative analysis of pelvic ligaments: a biomechanics study. Int Urogynecol J. 2013;24:135–9. https://doi.org/10.1007/s00192-012-1861-5.
22. Jelen K, Herman H, Lopot F, Kubovy P, Otcenasek M, Sedlacek R. Women with incorrect pelvic floor statics: a biomechanical answer to the mechanical loading of the vagina-endopelvic fascia complex. Neuroendocrinol Lett. 2010;31:413–7.
23. Janda S. Biomechanics of the pelvic floor musculature [Ph. D. thesis]. Technische Universiteit Delft. 2006.
24. Ogden RW, Saccomandi G, Sgura I. Fitting hyperelastic models to experimental data. Comput Mech. 2004;34:484–502. https://doi.org/10.1007/s00466-004-0593-y.
25. Yeoh OH. Some forms of the strain energy function for rubber. Rubber Chem Technol. 1993;66:754–71. https://doi.org/10.5254/1.3538343.
26. Noakes KF, Pullan AJ, Bissett IP, Cheng LK. Subject specific finite elasticity simulations of the pelvic floor. J Biomech. 2008;41:3060–5. https://doi.org/10.1016/j.jbiomech.2008.06.037.
27. Barzegari M, Vahidi B, Safarinejad MR, Ebad M. A computational analysis of the effect of supporting organs on predicted vesical pressure in stress urinary incontinence. Med Biol Eng Compu. 2020;58:1079–89. https://doi.org/10.1007/s11517-020-02148-2.

28. Routzong MR, Chang C, Goldberg RP, Abramowitch SD, Rostaminia G. Urethral support in female urinary continence part 1: dynamic measurements of urethral shape and motion. International Urogynecol J. 2021;1–10. https://doi.org/10.1007/s00192-021-04765-3.
29. Pregazzi R, Sartore A, Bortoli P, Grimaldi E, Troiano L, Guaschino S. Perineal ultrasound evaluation of urethral angle and bladder neck mobility in women with stress urinary incontinence. BJOG. 2002;109:821–7. https://doi.org/10.1016/S1470-0328(02)01163-1.
30. Fuganti PE, Gowdy JM, Santiago NC. Obesity and smoking: Are they modulators of cough intravesical peak pressure in stress urinary incontinence? Int Braz J Urol. 2011;37:528–33. https://doi.org/10.1590/S1677-55382011000400013.

Publisher's note Springer Nature remains neutral with regard to jurisdictional claims in published maps and institutional affiliations.

Springer Nature or its licensor holds exclusive rights to this article under a publishing agreement with the author(s) or other rightsholder(s); author self-archiving of the accepted manuscript version of this article is solely governed by the terms of such publishing agreement and applicable law.